Waste Management 159 (2023) 146–153

Contents lists available at ScienceDirect

Waste Management

journal homepage: www.elsevier.com/locate/wasman

Production of H_2 and CNM from biogas decomposition using biosolids-derived biochar and the application of the CNM-coated biochar for PFAS adsorption

Savankumar Patel [a,b], Mojtaba Hedayati Marzbali [a,b], Ibrahim Gbolahan Hakeem [a,b], Ganesh Veluswamy [a,b], Nimesha Rathnayake [a,b], Kamrun Nahar [a,b], Shivani Agnihotri [a,b], David Bergmann [c], Aravind Surapaneni [b,c], Rajender Gupta [d], Abhishek Sharma [b,e], Kalpit Shah [a,b,*]

[a] Chemical and Environmental Engineering, School of Engineering, RMIT University, Melbourne, VIC 3000, Australia
[b] ARC Training Centre for the Transformation of Australia's Biosolids Resources, RMIT University, Bundoora, VIC 3083, Australia
[c] South East Water Corporation, Frankston, VIC 3199, Australia
[d] Department of Chemical and Materials Engineering, University of Alberta, Edmonton, AB T6G 2G6, Canada
[e] Department of Chemical Engineering, Manipal University Jaipur, Jaipur, Rajasthan 303007, India

ARTICLE INFO

Keywords:
Biosolids-biochar
Hydrogen
Biogas
Carbon nanomaterials
PFAS
Circular economy

ABSTRACT

Anaerobic digestion is a popular unit operation in wastewater treatment to degrade organic contaminants, thereby generating biogas (methane-rich gas stream). Catalytic decomposition of the biogas could be a promising upcycling approach to produce renewable hydrogen and sequester carbon in the form of carbon nanomaterials (CNMs). Biosolids are solid waste generated during the wastewater treatment process, which can be valorised to biochar via pyrolysis. This work demonstrates the use of biosolids-derived biochar compared with ilmenite as catalysts for biogas decomposition to hydrogen and CNMs. Depending on the reaction time, biosolids-derived biochar achieved a CH_4 and CO_2 conversion of 50–70 % and 70–90 % at 900 °C with a weight hourly space velocity (WHSV) of 1.2 $Lg^{-1}h^{-1}$. The high conversion rate was attributed to the formation of amorphous carbon on the biochar surface, where the carbon deposits acted as catalysts and substrates for the further decomposition of CH_4 and CO_2. Morphological characterisation of biochar after biogas decomposition revealed the formation of high-quality carbon nanospheres (200–500 nm) and carbon nanofibres (10–100 nm) on its surface. XRD pattern and Raman spectroscopy also signified the presence of graphitic structures with I_D/I_G ratio of 1.19, a reduction from 1.33 in the pristine biochar. Finally, the produced CNM-loaded biochar was tested for PFAS adsorption from contaminated wastewater. A removal efficiency of 79 % was observed for CNM-coated biochar which was 10–60 % higher than using biochar and ilmenite alone. This work demonstrated an integrated approach for upcycling waste streams generated in wastewater treatment facilities.

1. Introduction

The anaerobic digestion unit is an integral part of the wastewater treatment process, generating biogas as a valuable product. The annual production volume of biogas in Australian wastewater treatment plants (WWTPs) is around 95 Mm^3, mainly composed of methane and carbon dioxide with trace amounts of ammonia, carbon monoxide, and hydrogen sulphide (Persson et al., 2006). Typical biogas contains 50–75 % methane and 30–50 % carbon dioxide with an energy density of about 25 MJ/m^3 (Goswami et al., 2016). However, biogas generated in WWTPs is usually not used for high-grade applications due to lower production volume and contaminant-related challenges. Hence, most WWTPs equipped with anaerobic digestion unit either use the biogas in boilers to generate steam for internal heating or flare the biogas in stacks (Zhao et al., 2010). The flaring/combustion of methane-rich biogas can increase the global warming potential associated with CH_4 and CO_2 emissions (Gupta and Singh, 2012).

Meanwhile, biogas can be a valuable precursor to produce hydrogen

* Corresponding author at: Chemical and Environmental Engineering, School of Engineering, RMIT University, Melbourne, VIC 3000, Australia.
E-mail address: kalpit.shah@rmit.edu.au (K. Shah).

https://doi.org/10.1016/j.wasman.2023.01.037
Received 29 September 2022; Received in revised form 26 January 2023; Accepted 31 January 2023
Available online 8 February 2023

and advanced carbon materials through a chemical vapour deposition process (Kong et al., 2020; Saputri et al., 2020). In this context, the catalytic decomposition of biogas at moderate to high temperatures (600–900 °C) can yield hydrogen-rich syngas and solid carbon deposits in the form of carbon nanomaterials (CNMs) (Pinilla et al., 2017). Producing hydrogen from biogas can be an attractive alternative for high-end utilisation of WWTPs-produced biogas as the process helps sequester carbon and reduce CO_2 and CH_4-associated emissions. Carbon nanomaterials have many commercial applications, such as adsorbent, catalyst, energy storage, graphene or graphitic material production, drug delivery in biomedical applications, and composite additives, depending on their structure and surface properties (Ali et al., 2019; Gabal et al., 2020; Lin et al., 2019).

Several catalyst materials have been investigated for biogas decomposition with various methane conversion rates and hydrogen yields reported. Metal catalysts especially transition metals (group VIII) catalysts are the popular and widely used active phase component usually supported on metal oxides for biogas decomposition. For example, De Llobet et al. (2015a) studied the performance of Al_2O_3-supported Ni, Co, and Fe catalysts for biogas decomposition at 600–900 °C. The authors observed that the choice of metal active sites influence CH_4 and CO_2 conversion rates, carbon production and morphology, and catalysts stability. In a latter study by De Llobet et al. (2015b) Ni/Al_2O_3 catalysts showed high selectivity for producing a fishbone-like nanocarbon material and syngas. However, the main limitation of metal-based catalysts is the rapid deactivation of the catalyst due to severe carbon deposition largely affected by the nature of carbon formed during the decomposition reaction (Wang and Lu, 1998; Wang and Lu, 1999). In addition to the high costs of metal catalysts, sintering of metallic catalysts is prominent under the high temperature conditions of methane decomposition; hence, it can be challenging to regenerate metal-based catalysts (Wang and Lu, 1999; Du et al., 2018). Naturally occurring mineral-based catalysts, particularly Fe-containing mineral phases, have shown superior stability and activity at high temperatures for methane decomposition process (Li et al., 2011; Lumbers et al., 2022; Qian et al., 2020). However, they contaminate the produced CNM with iron oxides.

Carbon-based catalysts, despite having lesser catalytic activity when compared with metallic catalysts can overcome some of the challenges associated with metallic catalysts. For example, carbon catalysts can exhibit high thermal stability and resistance against deactivation. More so, it might not be essential to separate the produced CNM from carbonaceous catalyst material, and where the separation is desired, carbon-based catalyst can enhance the purity of the CNM as metal-induced contamination (such as metal carbides) can be greatly reduced during downstream CNM-exfoliation process. Carbon-based catalysts such as biochar, activated char, carbon black, ordered mesoporous carbon, hierarchical porous carbon, carbide-derived carbon, fullerenes, and graphite have widely been studied as catalysts for methane decomposition (Ashik et al. 2015). However, some of these carbonaceous materials such as mesostructured carbons, fullerenes, and graphite requires rigorous synthesis steps, and their precursors are generally from fossil sources which might limit the techno-economic attractiveness for large scale production and application in biogas decomposition. The production and use of cheap carbon materials such as biochar or activated char from waste biomass precursors have been evaluated as catalysts in catalytic biogas decomposition process (Harun et al., 2020; Patel et al., 2020). It was demonstrated by Liew et al. (2018) that the method of carbon-catalyst production such as physical vs chemical activation can affect their performance in methane conversion and syngas production. The favorable properties of biochar-based catalyst material for methane decomposition include specific surface areas, micropore volume, and oxygen-containing functional groups (R-COOH, R-OCO, R-OH, R = O), finely dispersed inherent metals components, and carbon structures. However, the dominating properties of biochar for hydrogen production from thermocatalytic methane/biogas decomposition is elusive suggesting the need for more fundamental mechanistic studies.

Per- and polyfluoroalkyl substances (PFAS) are groups of persistent fluorinated organic compounds with a hydrophobic carbon chain backbone and hydrophilic functional head group. They are usually classified into long-chain and short-chain compounds depending on the length of the carbon backbone. PFAS have been detected in many wastewater treatment effluents in substantial concentrations, and the increasingly stringent regulations on PFAS control demands that these toxic compounds be removed from wastewater before disposal to the environment. Adsorption is the prominent method to remove PFAS in aqueous streams by taking advantage of the high water-solids partition coefficient of common PFAS such as PFOA, PFHxA and PFOS. Carbon nanomaterials have good adsorption capacity for organic pollutants, including PFAS, in aqueous systems owing to many desirable adsorption properties such as anion exchange capacity, surface morphology, and surface functional groups (Bei et al., 2014; Yu et al., 2014). Low-cost solid adsorbents such as biochar and commercial activated carbon can remove PFASs through hydrophobic and electrostatic interactions (Hassan et al., 2020). The use of CNM-coated biochar as adsorbent material for the uptake of PFAS compounds in wastewater has limited investigations.

The current paper is an extension of our earlier research where we demonstrated the use of biosolids-derived biochar for methane decomposition to hydrogen (Patel et al., 2020). In this work, a two-step chemical vapour deposition process was carried out to decompose biogas components mainly methane and carbondioxide using biosolids-derived biochar produced via pyrolysis in an earlier step. The presence of CO_2 in the biogas stream is envisaged to bring about new reaction pathways in the decomposition process which may influence the performance of biosolids-biochar catalyst. In addition, the stripped carbon from the biogas which is finely deposited on the biochar catalyst can produce new material termed carbon nanomaterial-coated biochar which can have unique or similar features of carbon nano tubes for a range of application including adsorption. The specific objectives of the current study are to (a) examine and compare the effect of biosolids-derived biochar and ilmenite as a catalyst for the production of carbon nanomaterials and hydrogen from biogas decomposition and (b) study the application of biochar and CNM-coated biochar for removing PFASs from contaminated water. This work demonstrates the concept of circularity in wastewater industries for the effective and integrated utilisation of various products streams. First an in-house produced biochar from wastewater treatment residuals (biosolids) is employed on-site to convert AD-generated biogas into hydrogen fuel and CNMs; then the CNMs-laden biochar can be applied internally to remove PFAS from contaminated wastewater streams.

2. Materials and methods

2.1. Catalyst preparation

The dried biosolids sample was collected from Mt Martha Water Recycling Plant, South East Water Corporation, Melbourne, Australia. The as-received dried biosolids were ground to 100–300 μm particle sizes. The pre-treated biosolids were placed in a muffle furnace (Barnstead Thermolyne 30400) operating at 700 °C for three hours (holding time) to produce biochar. The furnace was then kept closed until it was cooled down naturally to room temperature. Afterwards, the biochar was collected and stored in a desiccator for characterization and further experiments. Ilmenite ($FeTiO_3$) was obtained from a local supplier. Both biochar and ilmenite were used as catalysts for biogas decomposition.

2.2. Experimental setup

Biogas decomposition is referred to as chemical vapour deposition (CVD) from here onwards in the remaining manuscript. The experiments were performed in a fluidised bed tubular quartz reactor with an internal

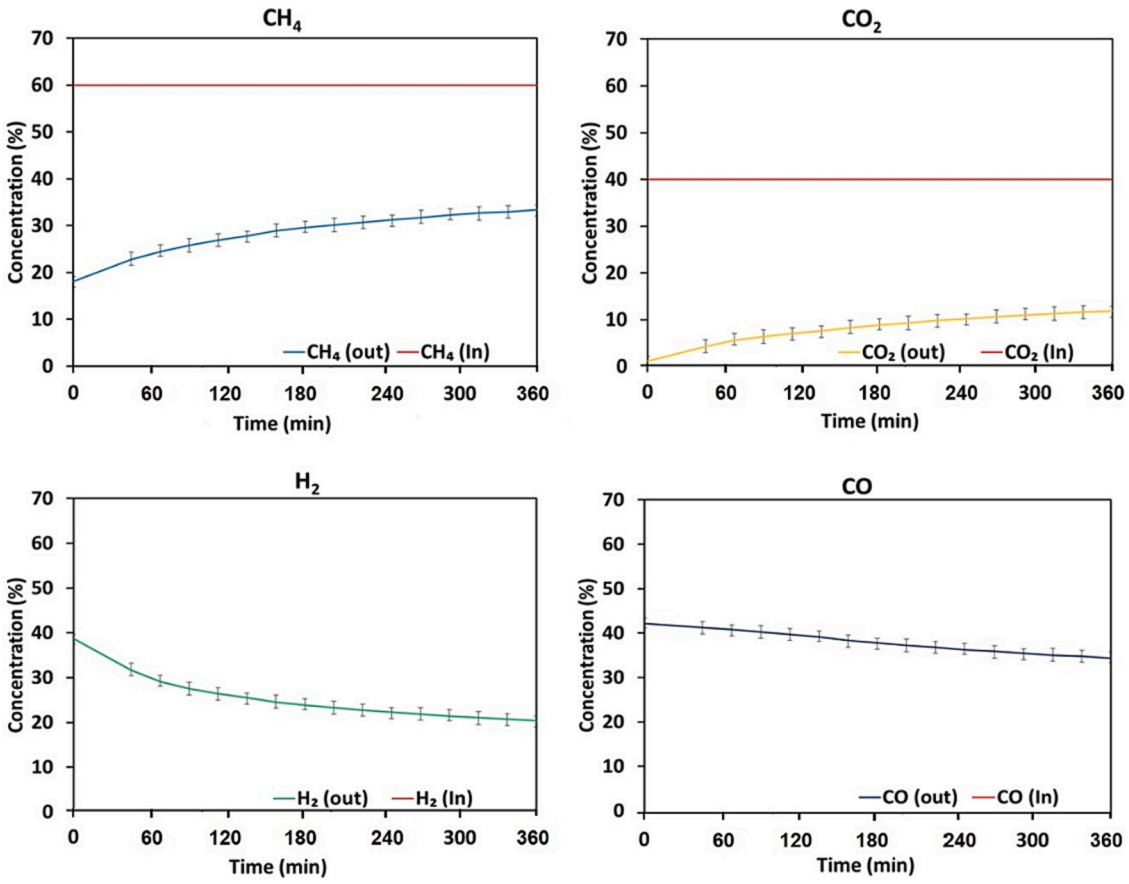

Fig. 1. Gas compositions from the CVD of biogas in the presence of biochar.

diameter of 27 mm and length of 650 mm heated by a three-zone electrical furnace. The experimental rig is illustrated in Fig. S1. Five grams of the fresh catalyst material, i.e., biochar or biochar-ilmenite mixture (1:1 on a weight basis), was loaded into the reactor, and the synthetic biogas (60 % CH_4, 40 % CO_2) was flowed at the rate of 100 mL min^{-1} through the bed to maintain a weight hourly space velocity (WHSV) at 1.2 $Lg^{-1}h^{-1}$. WHSV value is often in the range of 1 to 15 $Lg^{-1}h^{-1}$ (Abbas and Daud, 2010; Muradov et al., 2005). The CVD reactor was heated at the rate of 35 °C min^{-1}, then remained under isothermal condition at 900 °C for 6 h. Both solid and gas product streams were of interest in this study. The produced carbon material on the catalyst's surface (deposited carbon) was collected after cooling the reactor to room temperature under N_2 flow at 50 mL min^{-1}. Each experiment was replicated three times. Therefore, the data presented in this work represents the average values of three experimental data obtained under the same conditions.

2.3. Product analyses

The gases produced from the experiment were analysed using an online micro-GC (Agilent, micro-GC 490) instrument. The gases were extracted by micro-GC every 4 min for the analysis. The micro-GC was calibrated using standard calibration gases and details of calibration gases is given in Table S1. Then, this calibration was used to determine the components of the CVD gas and its composition (vol%). Scanning electron microscopy (SEM) imaging of deposited carbon samples was performed using an FEI Verios 460L instrument. Transmission Electron Microscopy (TEM) analysis was carried out using a JEOL-1010 microscope. For TEM analysis, the samples were finely ground and dispersed in isopropyl alcohol, and a drop of this solution was then inserted into a classical TEM carbon grid. X-Ray Diffraction (XRD) spectroscopic analysis was performed using a Bruker Axs D4 Endeavor Wide Angle XRD instrument fitted with a copper tube (Cu Kα radiation) from 6 to 90°. A Perkin-Elmer Raman Station 400F instrument was used for Raman spectroscopic analysis of carbon deposited on biochar samples.

2.4. PFAS adsorption

The carbon nanomaterials produced via the CVD process using biochar and ilmenite as catalysts were used to remove PFAS from wastewater. The adsorption capacity was also compared with a commercial granular activated carbon (GAC). PFASs contaminated trade wastewater samples were initially filtered through a 6-μm polyethersulfone membrane filter paper to remove any suspended solids. Four adsorbents were employed to remove PFASs from the contaminated water: 1) biosolids biochar, 2) CNM produced from CVD on biochar, 3) CNM produced from CVD on biochar and ilmenite mixture, and 4) GAC. For each study, one gram of adsorbent was taken in a conical flask, and 50 mL of PFAS-contaminated water was introduced into the conical flask. The PFAS-contaminated water contains PFOS, PFOA, and PFHxS and their concentrations are 310, 25, and 140 μg/L respectively. The conical flask was sealed, wrapped with aluminium foil, and placed in an orbital shaker (Thermoline TS-400). The mixture was agitated at 180 rpm for 48 h (Gagliano et al., 2020). Afterwards, the mixture was filtered using 0.45-μm polyethersulfone membrane filter paper to recover the adsorbent materials. The filtrate and raw wastewater were analysed for PFAS. The PFAS analysis was performed externally at ALS Water Resource Group, Melbourne, Australia (EPA 2022). The PFAS removal efficiency of the four adsorbent materials was determined using the concentration data before and after the adsorption.

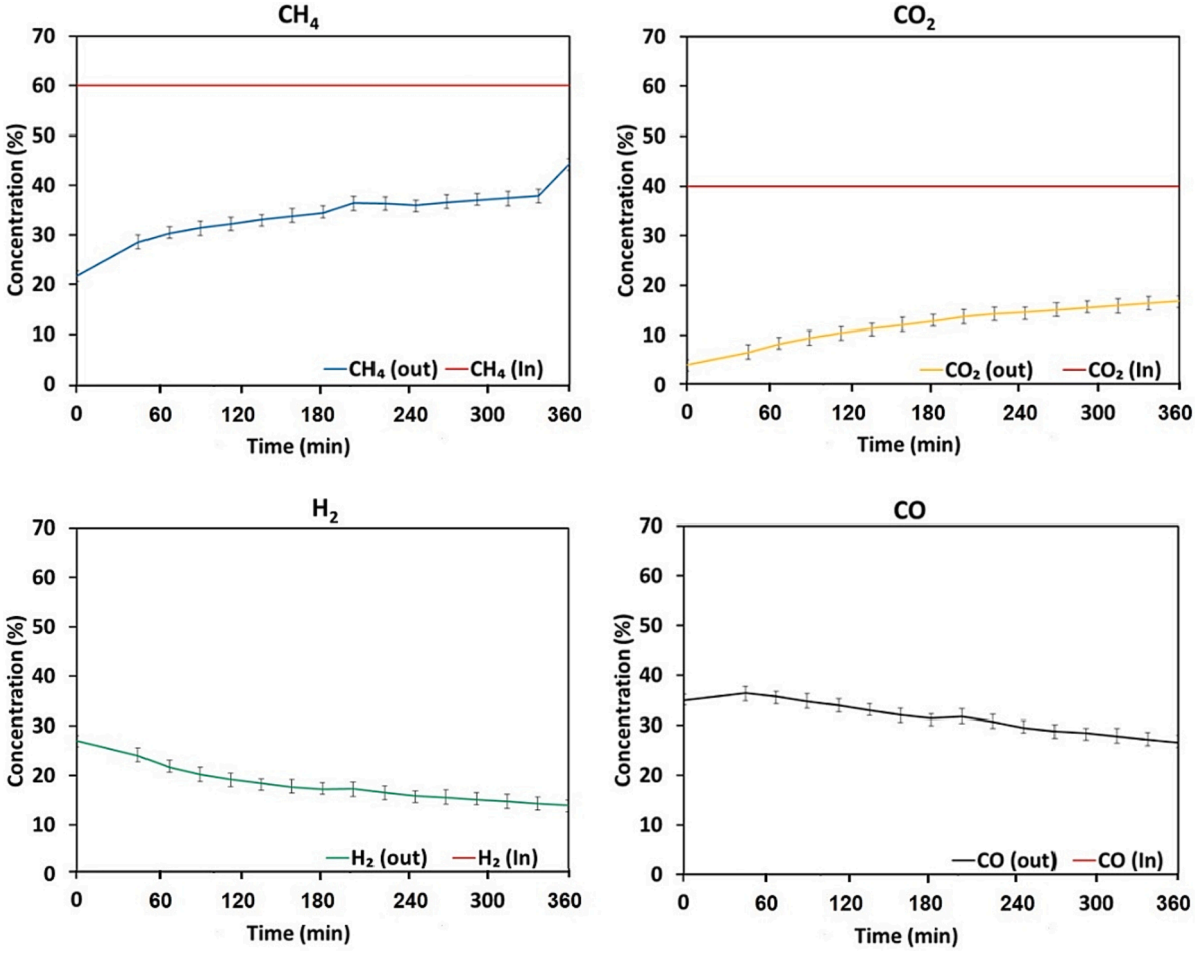

Fig. 2. Gas compositions from CVD of biogas in the presence of biochar-Ilmenite mixture.

3. Results and discussions

3.1. Gas product analysis

Fig. 1 illustrates the CVD gas profiles in the presence of biochar as the catalyst. It is observed that biochar converts CH_4 and CO_2 into syngas, i.e., hydrogen and carbon monoxide. The maximum methane conversion is observed in the first 30 min (~70 %), after which it dropped to a steady value of ~ 40 %. This trend is also reflected in the hydrogen concentration, which dropped from 40 % at the beginning of the process to 25 % after 6 h. The other main constituent of biogas, i.e., CO_2, is converted into CO in the first 30 min, and then the conversion remains constant at a value of ~ 65 % for the rest of the process. The following reactions (Equations 1–3) are assumed to occur during the decomposition of biogas into carbon and syngas in the presence of biochar.

$$CH_4 + CO_2 \leftrightarrow 2H_2 + 2CO \quad (1)$$

$$CH_4 \rightarrow C + 2H_2 \quad (2)$$

$$C + CO_2 \leftrightarrow 2CO \quad (3)$$

The higher initial conversion of methane can be attributed to the presence of fresh active sites of porous biochar containing carboxylic groups (Figueiredo 2013; Stein et al., 2009; Patel et al., 2020). At high temperatures (i.e., 900 °C), the carboxylic groups in biochar were initially decomposed to CO and CO_2, forming more active sites for methane molecule adsorption (Szymański et al., 2002; Patel et al., 2020). Also, the amorphous carbon present in biochar reacted with CO_2 to form CO through the Boudouard reaction (Equation (3)) prevalent at higher temperatures (>850 °C) (Lahijani et al., 2015), leading to the formation of more vacant active sites. As active sites were occupied with carbon deposits through decomposition reaction (Equation (2)), reactivity declined rapidly. However, the conversion values were stable for an extended period despite the increased carbon deposits. This might be due to the higher catalytic activity of new crystalline carbon deposits formed during the cracking (Patel et al., 2020; Shah et al., 2022). The crystallinity of carbon deposits formed on the catalyst might play a critical role in achieving stable conversions for an extended period, as crystalline carbon may act as a surrogate catalyst in the decomposition reaction (Patel et al., 2020). The overall methane conversion during the 6-hour reaction time was 50 %, while the corresponding average H_2 production was 30 %. As envisaged earlier, it is feasible to conduct the CVD process in the presence of biochar acting as a carbon precursor to produce high-value syngas and CNMs.

Fig. 2 compares the methane and CO_2 conversion rates for a mixture of biochar and ilmenite. The CH_4 and CO_2 conversion trends were observed to be similar to that in the presence of biochar alone, however, at a relatively lower conversion rate. Methane conversion rate dropped from a maximum of 60 % to 30 % during the 6-hour reaction time, while the CO_2 conversion rate declined from 90 % to 60 %. The overall CH_4 conversion during the CVD process on a mixture of biochar and ilmenite catalyst was 39 %, which is much lower than in the presence of biochar alone (~50 %). Lower H_2 production (~20 %) was also observed when the CVD process was conducted in the presence of a biochar-ilmenite catalyst. The difference in the methane conversion rates can be attributed to limited amorphous carbon-free active sites and different reaction pathways for Fe-based ilmenite in the mixture. Zhou et al. (2017)

Table 1
Comparison of methane conversion in CVD process under different catalysts.

Time (h)	Biochar (%)	Biochar + ilmenite (%)	Ni-Al_2O_3 (%)	Ni-Al_2O_3 (%)	Ni:Co (%)
Reference	This study	This study	(Pinilla et al., 2011)	(Pinilla et al., 2011)	(Pinilla et al., 2011)
First 10 min	70	64	75	68	64
1	59	49	68	43	47
2	56	44	65	38	40
3	53	41	59	35	34
4	47	38	–		
5	45	36	–		
6	44	25	–		

studied the catalytic methane decomposition process for different Fe-based catalysts and demonstrated that the process starts with the formation of Fe_3C and graphite simultaneously. As soon as Fe_3C is formed, it acts as a catalyst and promotes methane decomposition into H_2 and carbon. The carbon diffuses into Fe_3C to form supersaturated Fe_3C_{1+X}, which is unstable and immediately decomposes back to stoichiometric Fe_3C and graphite carbon.

The biogas methane conversion rates are summarised and compared in Table 1, along with other metal-based catalyst conversion data. As highlighted in the introduction section, metal-based catalysts, such as Ni-Al_2O_3 and Ni-Co can provide higher biogas methane conversion rates. However, it has disadvantages, such as high cost, low stability at high temperatures and sintering, and difficulty in regeneration (Pinilla et al., 2011). On the contrary, the biochar obtained from biosolids can be a sustainable alternative, as it presents many unique advantages over conventional metal-based catalysts. Biochar can act as carbon precursor by releasing carbon in the CVD reaction (Shah et al., 2022). Biochar can also act as a catalyst due to the fine dispersion of catalytically active metals in its porous matrix structure and can provide a substrate for the growth of CNMs.

3.2. Characterisation of solid product

3.2.1. SEM and TEM

The SEM and TEM images of biochar and biochar-ilmenite mixture along with carbon deposits after the CVD experiment helped identify the nature of carbon deposits. Fig. 3 shows the SEM and TEM images of spent biochar and the biochar-ilmenite mixture obtained after the CVD experiment at 900 °C. Carbon nanospheres (CNSs) with a uniform diameter of 200–500 nm were found to be deposited on both catalyst surfaces at 900 °C, as shown in Fig. 3 (a), (b), (d), and (e). They were highly curved and randomly tangled into each other. However, some CNSs aggregation was also noted due to their smaller diameter. Short-length carbon nanofibers (CNFs) aggregates with a diameter of 10–100 nm were also found to be deposited on biochar-ilmenite mixture surfaces at 900 °C, as shown in Fig. 3 (c) and (f).

3.2.2. XRD analysis

The XRD pattern in Fig. 4 shows the degree of graphitisation of CNMs formed on the catalyst's surface during the CVD of biogas. There was a steep increase in peak intensity at I_{002} on the biochar surface after CVD compared to a mixture of biochar and ilmenite. This peak was easily distinguishable from the peak observed for biochar alone when no CVD was conducted. Peaks at a 2θ angle of ~ 26.4° corresponding to the lattice plane I_{002} represent the presence of graphite structure (Mishra et al., 2012). This increase in the diffraction peak intensity at I_{002} indicates a higher degree of graphitisation and increase in crystallinity (Chen et al., 2008). The similar peak for biochar-ilmenite mixture is not as strong as for biochar alone. Methane decomposes to H_2 and amorphous carbon on the Fe° surface to form Fe_3C and a spurt of graphite carbon in less than 0.11 s (Sharma et al., 2009). Depending on the Fe-based catalyst composition, Fe_3C peaks occur between 37° and 47° (Zhou et al., 2017). Hence, the available free carbon from methane in biogas gets distributed as graphite and Fe_3C during CVD in the presence of biochar-ilmenite mixture. In Fig. 4, the Fe_3C peak is observed as a distinct peak at 37° in the biochar-ilmenite mixture.

Carbon nanotube structures are formed from multiple layers of pure graphene sheets with a thickness of about 0.335 nm, corresponding to the thickness of one carbon atom or the distance between two layers of

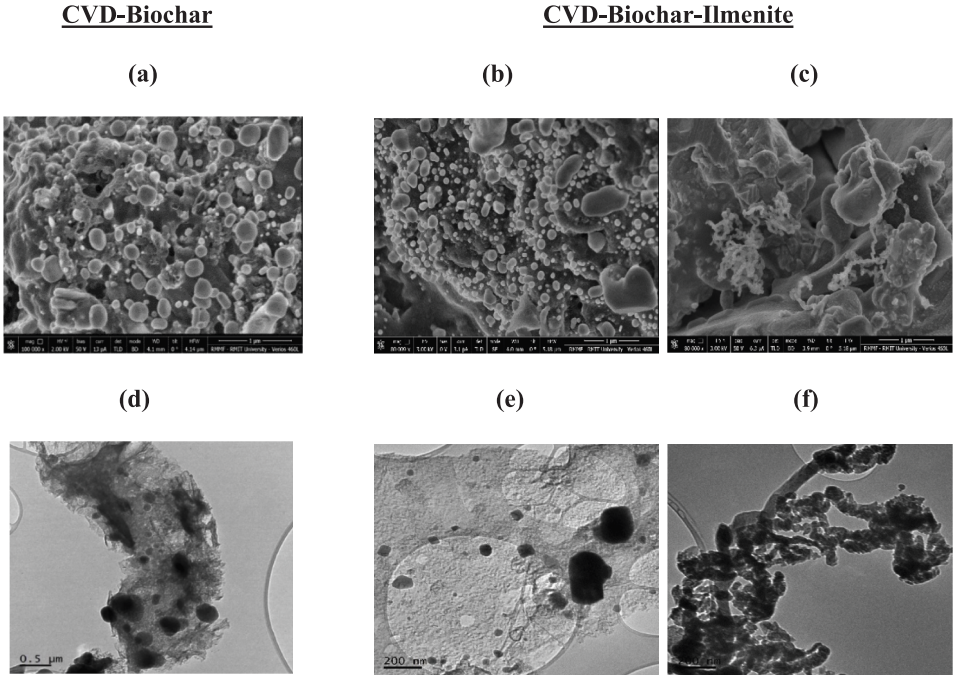

Fig. 3. SEM (a-c) and TEM (d-f) images of carbon nanomaterials formed on the surface of catalysts, i.e., biochar and biochar-ilmenite mixture after CVD process.

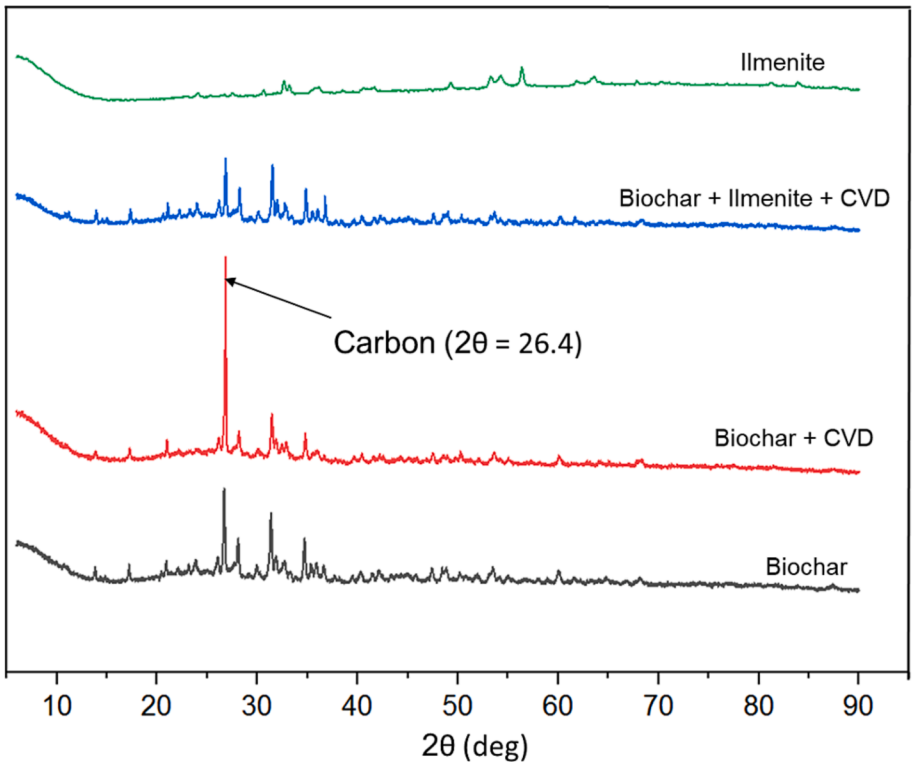

Fig. 4. XRD patterns of different catalysts before and after CVD process.

Table 2
Comparative analysis of crystallinity and degree of graphitization of different catalysts.

	Biochar	Biochar + CVD	Biochar + ilmenite + CVD
I_D/I_G	1.33	1.19	1.22

graphene in graphite (Wang et al., 2020). The interlayer spacing also termed d-spacing (d_{002}), values of the major graphite peak (I_{002}) were in the range of 0.334 to 0.335 nm in Fig. 4, confirming the formation of typical graphite structure (0.335 nm). This indicates that biochar surface acts as a substrate to aid the formation of high-quality carbon structure deposits during CVD.

3.2.3. *RAMAN spectroscopy*

Raman spectroscopy was employed to study the graphitization and crystallinity of the deposited CNMs (Table 2). Bands in the Raman spectrum were designated as the D, G, 2D, 2D‟ bands that emerged at ~1328, ~1598, ~2598 and 2936 cm^{-1}, respectively. These bands are the signatures of graphitic carbon (Pudukudy et al., 2017). D band indicates the presence of structural disorders or imperfections on the graphitic layers. G band is ascribed to the presence of carbon–carbon stretching vibration of the sp2 orbital in the graphitic layers of the CNMs (Kameya and Hanamura, 2011). 2D bands are associated with the formation of graphene layers in the CNMs (Pudukudy et al., 2017), while a low-intensity 2D band relative to the G band indicates few-layered graphene sheets (Dong et al., 2015).

Furthermore, the intensity ratio of D and G bands was calculated to evaluate the defect density and crystallinity and degree of graphitization of the carbon nanomaterial (Table 2). I_D/I_G value was found to be 1.33 for pristine biochar, while it marginally decreased to 1.19 and 1.22 for the carbon deposited over the biochar catalyst and biochar-Ilmenite mixture, respectively. This can demonstrate a lower defect density in the samples after the CVD process, suggesting the formation of a graphitic structure. In Fig. 5, distinct 2D peaks with a relatively low

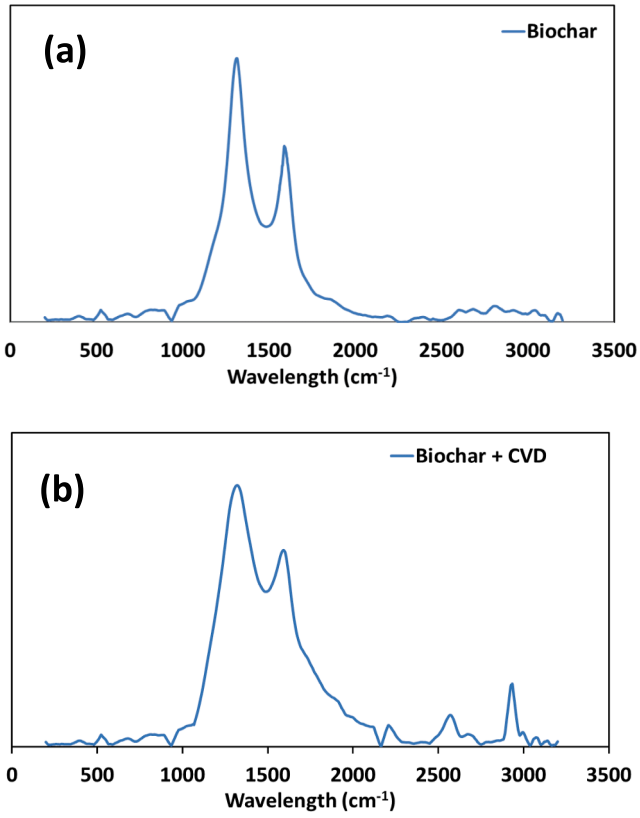

Fig. 5. Raman spectra of the carbon deposited over (a) biochar and (b) Biochar after CVD.

Table 3
PFAS concentration in the treated filtrate and adsorption efficiency by various samples.

Sample	PFOS (μg/L)	PFOA (μg/L)	PFHxS (μg/L)	Removal efficiency (%)			
				PFOS	PFOA	PFHxS	Average
Wastewater	310	25	140	–	–	–	–
Biochar	38	9.7	50	88	61	64	71
CVD-Biochar	17	7.3	39	95	71	72	79
Ilmenite	110	19	130	65	24	7	32
CVD-Biochar-Ilmenite	43	14	97	86	44	31	54
GAC	0.52	0.07	0.18	100	100	100	100

intensity compared to G band can be observed for pristine biochar samples and after CVD. This indicates the occurrence of graphene layers on the sample surface.

3.3. PFAS adsorption

Table 3 shows the removal efficiency of PFASs compounds from sample wastewater using different adsorbents, including CNMs produced from the CVD process. The concentration of PFAS in the sample water was 310 μg/L (PFOS), 25 μg/L (PFOA) and 140 μg/L (PFHxS). GAC had an efficiency of 100 % in removing the PFASs compounds in the water sample. The surface area and pore diameter of the adsorbent materials are given in Table S2. The adsorption of PFASs by GAC is a slow process, and it can take up to 2–3 days or even longer, to reach adsorption equilibrium (Chen et al., 2011). It is one of the several problems of utilising GAC commercially in wastewater treatment facilities (Liu et al., 2020). Recently, researchers have shown that some smaller chain PFASs, may penetrate through GAC and get adsorbed faster than their longer chain equivalents. Also, GAC optimized for PFOS removal may not optimally remove other PFAS compounds (Rayne and Forest, 2009). Carbon nanomaterial produced during the CVD process using the biosolids-derived biochar was found to have properties similar to CNTs. CNMs, especially CNTs, possess a high specific surface area, porosity, anion-cation adsorption capacity, and chemical and thermal stability (Kumar et al., 2017). CNMs are advantageous over the conventional PFASs adsorbents in terms of reusing the adsorbent after regeneration, having a better adsorption capacity and easy functionalization (Deng et al., 2013). This suggests that CNM produced in this study might have the potential to demonstrate higher sorption capacity for PFASs.

A relatively high PFAS removal efficiency of 79 % was observed for CNM-coated biochar containing carbon nanospheres of 1 μm, whereas it was 71 % removal efficiency for biochar alone. Chen et al. (2011) investigated the removal of PFASs with CNTs, char and ash. They found that CNTs demonstrate high sorption capacity compared to char and ash due to the high available active spaces on the cylindrical external surface. The purity of the CNT also plays an important role (Li et al., 2012). CNMs extracted from biochar showed an I_D/I_G ratio of 1.19 in the Raman Spectroscopy analysis, indicating a purer graphitic structure. Therefore, higher PFASs removal efficiency was achieved by CNM-loaded biochar. Ilmenite and its CVD-derived CNM had the lowest removal efficiency of PFASs perhaps due to its non-graphitic structure as shown in Fig. 6. The recent advances in science have enabled researchers to functionalise CNMs surface to introduce new adsorption sites and change its hydrophobic, hydrophilic or amphiphilic properties, enabling them to perform better compared to the conventional adsorbents. Therefore, given the ability of CNMs to achieve equilibrium within a short duration and their high PFASs removal efficiency, it can be a long-term alternative to GAC.

4. Limitations and recommendations for future work

- It has been observed that carbon nanomaterial and hydrogen can be produced from biogas decomposition using biosolids-derived biochar as a catalyst. However, optimisation of process parameters, such as effect of WHSV and temperature on the decomposition performance of biochar has not been investigated. The quality and growth of CNMs as well as hydrogen yield can be controlled by optimising these parameters. Hence future works should explore this critical gap in this research.
- The solid product (carbon nanomaterial coated biochar) was tested for PFAS removal from contaminated wastewater in a batch adsorption process. The material demonstrated good PFAS adsorption capacity which can be attractive for further development. However, fundamental investigation of the adsorption process involving mass transfer limitations, governing mechanisms, and reaction kinetics as well as performance in continuous process are necessary. This will enhance the development of industrially viable adsorbent for PFAS removal from contaminated waste streams.
- In this study, the focus was to produce carbon nanomaterial loaded biochar which was tested for PFAS removal from contaminated wastewater without prior separation or purification steps. The recovery and purity of the deposited carbon nanomaterial after separation from the biochar using electro-chemical or ultra-sonication methods is recommended for future works. Lastly, it is important to study the performance of the material in other potential high-end applications such as energy storage devices, biomedicals, and catalysis.

5. Conclusions

Catalytic decomposition of biogas was investigated using biochar and biochar-ilmenite mixture at 900 °C. The overall methane decomposition and CO_2 conversion rates were observed to be reasonably higher in the presence of biochar. In the case of the Fe-based catalyst (ilmenite), the carbon in methane is distributed into graphitic carbon and Fe_3C, leading to limited active sites. The crystallinity of carbon deposits was higher for biochar than the Fe-based catalyst, demonstrating better performance stability and, thus, higher conversion. CNMs-loaded biochar demonstrated a higher PFASs removal efficiency of 79 %, compared to the biochar-ilmenite mixture (54 %). Hence, biosolids-derived biochar could be a long-term alternative to activated carbon and metal-based catalysts limited by their costs and need for constant regeneration. Biochar can potentially provide much-needed sustainability to wastewater industries when integrated with solid and gas product stream lines.

Declaration of Competing Interest

The authors declare that they have no known competing financial interests or personal relationships that could have appeared to influence the work reported in this paper.

Data availability

Data will be made available on request.

Appendix A. Supplementary material

Supplementary data to this article can be found online at https://doi.org/10.1016/j.wasman.2023.01.037.

References

Abbas, H.F., Daud, W.W., 2010. Influence of reactor material and activated carbon on the thermocatalytic decomposition of methane for hydrogen production. Appl. Catal. A: Gen. 388, 232–239.

Ali, I., Kucherova, A., Memetov, N., Pasko, T., Ovchinnikov, K., Pershin, V., Kuznetsov, D., Galunin, E., Grachev, V., Tkachev, A., 2019. Advances in carbon nanomaterials as lubricants modifiers. J. Mol. Liq. 279, 251–266.

Ashik, U.P.M., Wan Daud, W.M.A., Abbas, H.F., 2015. Production of greenhouse gas free hydrogen by thermocatalytic decomposition of methane – A review. Renew. Sustain. Energy Rev. 44, 221–256.

Bei, Y., Deng, S., Du, Z., Wang, B., Huang, J., Yu, G., 2014. Adsorption of perfluorooctane sulfonate on carbon nanotubes: influence of pH and competitive ions. Water Sci. Technol. 69, 1489–1495.

Chen, X., Xia, X., Wang, X., Qiao, J., Chen, H., 2011. A comparative study on sorption of perfluorooctane sulfonate (PFOS) by chars, ash and carbon nanotubes. Chemosphere 83, 1313–1319.

Chen, Y., Riu, D.-H., Lim, Y.-S., 2008. Carbon nanotubes grown over Fe− Mo− Mg− O composite catalysts. Met. Mater. Int. 14, 385–390.

De Llobet, S., Pinilla, J.L., Moliner, R., Suelves, I., 2015a. Relationship between carbon morphology and catalyst deactivation in the catalytic decomposition of biogas using Ni, Co and Fe based catalysts. Fuel 139, 71–78.

De Llobet, S., Pinilla, J., Moliner, R., Suelves, I., 2015b. Effect of the synthesis conditions of Ni/Al2O3 catalysts on the biogas decomposition to produce H2-rich gas and carbon nanofibers. Applied Catal. B: Environ. 165, 457–465.

Deng, S., Niu, L., Bei, Y., Wang, B., Huang, J., Yu, G., 2013. Adsorption of perfluorinated compounds on aminated rice husk prepared by atom transfer radical polymerization. Chemosphere 91, 124–130.

Dong, L., Du, Y., Li, J., Wang, H., Yang, Y., Li, S., Tan, Z., 2015. The effect of CH4 decomposition temperature on the property of deposited carbon over Ni/SiO2 catalyst. Int. J. Hydrogen Energy 40, 9670–9676.

Du, J., Gao, J., Gu, F., Zhuang, J., Lu, B., Jia, L., Xu, G., Liu, Q., Su, F., 2018. A strategy to regenerate coked and sintered Ni/Al2O3 catalyst for methanation reaction. Int. J. Hydrogen Energy 43, 20661–20670.

EPA, 2022. PFAS EPA Draft Method 1633: Answers to six key questions. Washington, DC.

Figueiredo, J.L., 2013. Functionalization of porous carbons for catalytic applications. J. Mater. Chem. A 1, 9351–9364.

Gabal, E., Chatterjee, S., Ahmed, F.K., Abd-Elsalam, K.A., 2020. Carbon nanomaterial applications in air pollution remediation. Carbon Nanomater. Agri-Food Environ. Appl. 7, 133–153.

Gagliano, E., Sgroi, M., Falciglia, P.P., Vagliasindi, F.G., Roccaro, P., 2020. Removal of poly-and perfluoroalkyl substances (PFAS) from water by adsorption: Role of PFAS chain length, effect of organic matter and challenges in adsorbent regeneration. Water Res. 171, 1–31.

Goswami, R., Chattopadhyay, P., Shome, A., Banerjee, S.N., Chakraborty, A.K., Mathew, A.K., Chaudhury, S., 2016. An overview of physico-chemical mechanisms of biogas production by microbial communities: a step towards sustainable waste management. 3 Biotech 6, 1-12.

Gupta, D., Singh, S.K., 2012. Greenhouse gas emissions from wastewater treatment plants: a case study of Noida. J. Water Sust. 2, 131–139.

Harun, K., Adhikari, S., Jahromi, H., 2020. Hydrogen production via thermocatalytic decomposition of methane using carbon-based catalysts. RSC Adv. 10, 40882–40893.

Hassan, M., Liu, Y., Naidu, R., Du, J., Qi, F., 2020. Adsorption of Perfluorooctane sulfonate (PFOS) onto metal oxides modified biochar. Environ. Technol. Innov. 19, 100816.

Kameya, Y., Hanamura, K., 2011. Kinetic and Raman spectroscopic study on catalytic characteristics of carbon blacks in methane decomposition. Chem. Eng. J. 173, 627–635.

Kong, F., Swift, J., Zhang, Q., Fan, L.-S., Tong, A., 2020. Biogas to H2 conversion with CO2 capture using chemical looping technology: Process simulation and comparison to conventional reforming processes. Fuel 279, 118479.

Kumar, S., Rani, R., Dilbaghi, N., Tankeshwar, K., Kim, K.-H., 2017. Carbon nanotubes: a novel material for multifaceted applications in human healthcare. Chem. Soc. Rev. 46, 158–196.

Lahijani, P., Zainal, Z.A., Mohammadi, M., Mohamed, A.R., 2015. Conversion of the greenhouse gas CO2 to the fuel gas CO via the Boudouard reaction: A review. Renew. Sustain. Energy Rev. 41, 615–632.

Li, C., Schäffer, A., Séquaris, J.-M., László, K., Tóth, A., Tombácz, E., Vereecken, H., Ji, R., Klumpp, E., 2012. Surface-associated metal catalyst enhances the sorption of perfluorooctanoic acid to multi-walled carbon nanotubes. J. Colloid Interface Sci. 377, 342–346.

Li, Y., Li, D., Wang, G., 2011. Methane decomposition to COx-free hydrogen and nanocarbon material on group 8–10 base metal catalysts: a review. Catal. Today 162, 1–48.

Liew, R.K., Chong, M.Y., Osazuwa, O.U., Nam, W.L., Phang, X.Y., Su, M.H., Cheng, C.K., Chong, C.T., Lam, S.S., 2018. Production of activated carbon as catalyst support by microwave pyrolysis of palm kernel shell: a comparative study of chemical versus physical activation. Res. Chem. Intermed. 44, 3849–3865.

Lin, Z., Wu, G., Zhao, L., Lai, K.W.C., 2019. Carbon nanomaterial-based biosensors: A review of design and applications. IEEE Nanotechnol. Magazine 13, 4–14.

Liu, L., Liu, Y., Gao, B., Ji, R., Li, C., Wang, S., 2020. Removal of perfluorooctanoic acid (PFOA) and perfluorooctane sulfonate (PFOS) from water by carbonaceous nanomaterials: A review. Crit. Rev. Environ. Sci. Technol. 50, 2379–2414.

Lumbers, B., Agar, D.W., Gebel, J., Platte, F., 2022. Mathematical modelling and simulation of the thermo-catalytic decomposition of methane for economically improved hydrogen production. Int. J. Hydrogen Energy 47, 4265–4283.

Mishra, N., Das, G., Ansaldo, A., Genovese, A., Malerba, M., Povia, M., Ricci, D., Di Fabrizio, E., Di Zitti, E., Sharon, M., 2012. Pyrolysis of waste polypropylene for the synthesis of carbon nanotubes. J. Anal. Appl. Pyrolysis 94, 91–98.

Muradov, N., Smith, F., Ali, T., 2005. Catalytic activity of carbons for methane decomposition reaction. Catal. Today 102, 225–233.

Patel, S., Kundu, S., Halder, P., Marzbali, M.H., Chiang, K., Surapaneni, A., Shah, K., 2020. Production of hydrogen by catalytic methane decomposition using biochar and activated char produced from biosolids pyrolysis. Int. J. Hydrogen Energy 45, 29978–29992.

Persson, M., Jönsson, O., Wellinger, A., 2006. Biogas upgrading to vehicle fuel standards and grid injection. IEA Bioenergy task 1–34.

Pinilla, J.L., De Llobet, S., Suelves, I., Utrilla, R., Lázaro, M.J., Moliner, R., 2011. Catalytic decomposition of methane and methane/CO2 mixtures to produce synthesis gas and nanostructured carbonaceous material. Fuel 90, 2245–2253.

Pinilla, J., De Llobet, S., Moliner, R., Suelves, I., 2017. Ni-Co bimetallic catalysts for the simultaneous production of carbon nanofibres and syngas through biogas decomposition. Appl. Catal. B: Environ. 200, 255–264.

Pudukudy, M., Yaakob, Z., Mazuki, M.Z., Takriff, M.S., Jahaya, S.S., 2017. One-pot sol-gel synthesis of MgO nanoparticles supported nickel and iron catalysts for undiluted methane decomposition into COx free hydrogen and nanocarbon. Appl. Catal. B: Environ. 218, 298–316.

Qian, J.X., Chen, T.W., Enakonda, L.R., Liu, D.B., Mignani, G., Basset, J.-M., Zhou, L., 2020. Methane decomposition to produce COx-free hydrogen and nanocarbon over metal catalysts: A review. Int. J. Hydrogen Energy 45, 7981–8001.

Rayne, S., Forest, K., 2009. Perfluoroalkyl sulfonic and carboxylic acids: A critical review of physicochemical properties, levels and patterns in waters and wastewaters, and treatment methods. J. Environ. Sci. Health Part A 44, 1145–1199.

Saputri, D., Jan'ah, A., Saraswati, T., 2020. Synthesis of Carbon Nanotubes (CNT) by Chemical Vapor Deposition (CVD) using a biogas-based carbon precursor: A review, IOP Conference Series: Mater. Sci. Eng. IOP Publishing, p. 012019.

Shah, K., Patel, S., Halder, P., Kundu, S., Marzbali, M.H., Hakeem, I.G., Pramanik, B.K., Chiang, K., Patel, T., 2022. Conversion of pyrolytic non-condensable gases from polypropylene co-polymer into bamboo-type carbon nanotubes and high-quality oil using biochar as catalyst. J. Environ. Manage. 301, 113791.

Sharma, R., Moore, E., Rez, P., Treacy, M.M., 2009. Site-specific fabrication of Fe particles for carbon nanotube growth. Nano Lett. 9, 689–694.

Stein, A., Wang, Z., Fierke, M.A., 2009. Functionalization of Porous Carbon Materials with Designed Pore Architecture. Adv. Mater. 21, 265–293.

Szymański, G.S., Karpiński, Z., Biniak, S., Swiatkowski, A., 2002. The effect of the gradual thermal decomposition of surface oxygen species on the chemical and catalytic properties of oxidized activated carbon. Carbon N. Y. 40, 2627–2639.

Wang, S., Lu, G., 1998. Reforming of methane with carbon dioxide over Ni/Al2O3 catalysts: Effect of nickel precursor. Appl. Catal. A: Gen. 169, 271–280.

Wang, S., Lu, G., 1999. A comprehensive study on carbon dioxide reforming of methane over Ni/γ-Al2O3 catalysts. Ind. Eng. Chem. Res. 38, 2615–2625.

Wang, X., Sharif, F., Liu, X., Licht, G., Lefler, M., Licht, S., 2020. Magnetic carbon nanotubes: Carbide nucleated electrochemical growth of ferromagnetic CNTs from CO2. J. CO2 Util. 40, 101218.

Yu, J.-G., Zhao, X.-H., Yu, L.-Y., Jiao, F.-P., Jiang, J.-H., Chen, X.-Q., 2014. Removal, recovery and enrichment of metals from aqueous solutions using carbon nanotubes. J. Radioanal. Nucl. Chem. 299, 1155–1163.

Zhao, Q., Leonhardt, E., MacConnell, C., Frear, C., Chen, S., 2010. Purification technologies for biogas generated by anaerobic digestion. Compressed Biomethane, CSANR, Ed 24.

Zhou, L., Enakonda, L.R., Harb, M., Saih, Y., Aguilar-Tapia, A., Ould-Chikh, S., Hazemann, J.-L., Li, J., Wei, N., Gary, D., 2017. Fe catalysts for methane decomposition to produce hydrogen and carbon nano materials. Appl. Catal. B: Environ. 208, 44–59.